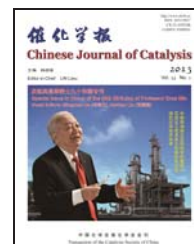available at www.sciencedirect.com

ScienceDirect

journal homepage: www.elsevier.com/locate/chnjc

Article

Synthesis of Ni/Mo/N catalyst and its application in benzene hydrogenation in the presence of thiophene

CHU Qi, FENG Jie*, LI Wenying, XIE Kechang

Key Laboratory of Coal Science and Technology, Taiyuan University of Technology, Taiyuan 030024, Shanxi, China

A R T I C L E   I N F O

A B S T R A C T

Ni/Mo/N catalysts made to have an interstitial structure gave high catalytic activity and sulfur tolerance in the hydrotreating of coal liquid fuel to produce high performance jet fuel. The dissolving of N atoms into the metal lattices to make the interstitial structure is difficult to control, and the preparation conditions of the precursor synthesis and the crystallinity of the precursors were changed to monitor how N atoms were inserted into the metal lattice. Ni/Mo/N catalysts were prepared by a one pot synthesis using ammonium molybdate $[(NH_4)_6Mo_7O_{24}\cdot4H_2O]$ and nickel acetate $[Ni(CH_3COO)_2\cdot4H_2O]$ and the decomposition of hexamine under an argon atmosphere at 650 °C. Benzene hydrogenation was used as a model reaction to evaluate catalytic activity. Benzene was hydrogenated over the Ni/Mo/N catalyst at 250 °C and 3 MPa in a fixed bed reactor in the absence and presence of thiophene to also test the Ni/Mo/N catalysts for sulfur tolerance. X-ray diffraction analysis showed that the formation of different precursors and use of different aging times affected the composition of the Ni/Mo/N catalysts, and also determined the crystal phases in the Ni/Mo/N catalysts. Ni_2Mo_3N, Mo_2C, and Ni metal phases were present in the most active Ni/Mo/N catalyst which gave a conversion of benzene of 93% and selectivity to cyclohexane of almost 100%. The atomic ratio of Ni/Mo in the most active Ni/Mo/N catalyst was 5/4 as determined by energy dispersive X-ray spectroscopy. Benzene hydrogenation over the Ni/Mo/N catalyst in the presence of thiophene led to a decline in benzene conversion from 72% to 50% due to the formation of MoS_2.

1. Introduction

The purpose of green chemistry is to develop atom economy and environment friendly processes [1]. In converting coal liquid oil to jet fuel and diesel fuel, a high aromatic hydrocarbon content in the coal liquid fuel adversely affects fuel quality and its hydrotreatment. The guidelines of the Environmental Protection Agency (EPA) specify that the aromatic content in jet fuel and diesel fuel is not to exceed 10 vol% [2,3]. Decreasing the amount of aromatics increase cetane numbers and improve the combustion characteristics, therefore, removing aromatics

from coal liquid fuel is one way to improve fuel quality and avoid environmental pollution. However, the high organic sulfur content in coal liquid oil places some limits on the oil hydrotreatment, such as obtainable catalytic activity, and feasible technical processing. Currently, noble metal catalysts and metal sulfide catalysts are used in the hydrodearomatization process in the coal and petrochemical industries. However, the advantages of noble metal catalysts [1,4] such as high activity and selectivity are limited by metal site poisoning. For the metal sulfide catalysts [5,6], the need to use harsh operating conditions increase both energy consumption and cost. Therefore,

the development of highly efficient and environment friendly catalysts is needed to meet the demand of green chemistry.

Ni/Mo/N bimetallic nitride catalysts have recently attracted considerable attention. In comparison with conventional catalysts such as Ni, Pt, and Pd, and Ni-Mo-S and Ni-W-S metal sulfide, they have higher catalytic activity and better sulfur resistance [7], which are particularly important for processing coal liquid fuels. Ni/Mo/N catalysts with an interstitial structure are produced by dissolving N atoms into the metal lattice. N atoms which enter the metal lattice occupy the largest interstitial sites available and change the structural and electronic properties of the non-noble metal such that it has catalytic properties similar to a noble metal catalyst [7]. In the synthesis of Ni/Mo/N catalysts with an interstitial structure, there is a possibility that non-metallic atoms will be lost from the solvent. Hence, it is challenging to control the process of getting N atoms into the metal lattice. Many researchers have modified this process using new preparation routes [8–13] to manage the crystallinity of the precursors and the calcination condition [11,14]. For example, Weil et al. [11] controlled the synthesis precursor and calcination temperature to manage the synthesis of nitrides. They analyzed the influence of additive amount and additive rate of triethylamine on the formation of the precursor ((N(C$_2$H$_5$)$_3$)·HCl), and the effects of high treatment temperature (950 °C) and long baking time (20 h) on the formation of the pure nitrides. The decomposition of hexamine (HMT) supplied H$_2$, N$_2$, and CH$_4$ at temperatures above 300 °C, so HMT as a source of nitrogen and carbon and as a reducing agent was used in the preparation of nitrides [12,14,15]. In another work, it was noticed that a high calcination temperature led to the loss of the doped atom. In yet another research paper, carbides were found to form when the calcination temperature was above 650 °C [16].

In this article, we focused on how to prepare the precursors so that they have crystal phases that are beneficial to the crystallization of the Ni/Mo/N catalyst. The effect of the precursor composition was investigated by changing the aging time of the precursors to understand the effect on the catalyst and its catalytic activity in the benzene hydrogenation. Thiophene is the major sulfur compound in coal liquid fuel and its presence will seriously decrease the activity of the metal nitride catalyst [17]. Therefore, the catalytic activity and sulfur tolerance of the catalysts were also evaluated by the benzene hydrogenation reaction with the adding of thiophene.

2. Experimental

2.1. Precursor synthesis

HMT forms a metal complex with Ni/Mo/Co/Mn nitrates, acetates and fluoroborates [18–20]. The precursors were prepared with Ni(CH$_3$COO)$_2$·4H$_2$O, (NH$_4$)$_6$Mo$_7$O$_{24}$·4H$_2$O, and HMT with the mole ratio of 14:3:34 [15]. (NH$_4$)$_6$Mo$_7$O$_{24}$·4H$_2$O and HMT were dissolved in 15% NH$_3$·H$_2$O in a 3:1 stoichiometric molar ratio (Mo:N). Ni(CH$_3$COO)$_2$·4H$_2$O and HMT were dissolved in 15% NH$_3$·H$_2$O in a higher than 2:1 stoichiometric molar ratio (Ni:N). Once the above materials were completely dis-

solved, the Mo/N solution was added to the Ni/N solution under stirring at either 300 or 450 r/min at 40 °C. The rate of addition of the Mo/N solution determined the formation of Ni/Mo/N. After the combined solution was evaporated to dryness, the precursors were aged for either 0 or 1 d. Then, the solids were dried at 80 °C for 6 hours.

2.2. Catalyst preparation

The precursors were calcined in Ar at a rate of 100 ml/min using the following sequence of heat treatment conditions: (1) ramp from room temperature to 50 °C in 10 min; (2) ramp from 50 to 150 °C at 3 °C/min; (3) ramp from 150 to 650 °C at 2 °C/min and kept at 650 °C for 2 h; (4) cooling the solid to room temperature. After calcination, the sample was passivated for 2 h in a flow of 1 vol% O$_2$/N$_2$. The Ni/Mo/N catalysts and their crystalline phases are listed in Table 1.

2.3. Chemical and structural characterization

The atomic ratio of Ni/Mo was determined by energy dispersive X-ray spectroscopy (EDX). The particles and exposed crystals of the catalysts were observed by transmission electron microscopy (TEM). The crystalline phase was detected by X-ray diffraction (XRD) carried out on a Rigaku diffraction instrument with Cu K_α radiation with the following step scan setting: 10°–90° range for catalysts, 5°–90° range for precursors, and 0.02° step length. The Debye-Scherer equation was used to calculate the particle size of the samples. The phase content was calculated by the reference intensity ratio (RIR) method. The surface compositions of the catalysts were measured with a ESCALAB 250 Xi spectrometer with a monochromatized Al source. The analyzer was operated with a constant pass energy (E_{pass} = 20.0 eV). The resolution measured on the Ag 3$d_{5/2}$ line was 0.5 eV.

2.4. Catalytic activity

Benzene was used as a model compound to evaluate the catalytic activity of the Ni/Mo/N catalysts. Using the conditions of 250 °C and 3 MPa in a fixed bed reactor, benzene hydrogenation was run in the absence and presence of thiophene. After

Table 1
Preparation conditions and crystalline phases of the Ni/Mo/N catalysts.

Catalyst	Addition means of Mo/N to Ni/N	Evaporation rate (r/min)	Aging time (d)		Crystalline phase
			Before drying	After drying	
A	Rapid	N/A	1	0	Ni$_2$Mo$_3$N; Mo$_2$C; MoO$_2$
B	Rapid	N/A	1	30	Ni$_2$Mo$_3$N; Ni; MoO$_2$
C	Slow	N/A	1	0	MoO$_2$; Ni
D	Rapid	N/A	0	0	Ni
E	Rapid	300	1	0	Ni$_2$Mo$_3$N; Mo$_2$C; Ni
F	Rapid	450	1	0	Ni$_3$C

The product concentrations were measured by gas chromatography (GC) with a 30 m capillary column (RTX-1) and an FID detector.

reaction, the catalysts were reduced for 2 h in H_2 at 500 °C. The mole ratio of H_2 to benzene was 4:1. When benzene hydrogenation was run in the presence of thiophene, the concentration of thiophene was 0.01 wt% in the solution of benzene and thiophene.

3. Results and discussion

3.1. Analysis of chemical and structural characterization

The crystalline phases of catalysts A, B, and C are shown in Fig. 1 and listed in Table 1. The difference between catalysts A and C was the addition rate of the Mo/N solution to the Ni/N solution. The Ni_2Mo_3N phase was not formed when the Mo/N solution was slowly added to the Ni/N solution (catalyst C), and the MoO_2 and Ni phases were detected. The phase contents were calculated by the RIR method, and the content of the Ni phase was almost 100%. A rapid addition of Mo/N to the Ni/N solution resulted in the formation of the Ni_2Mo_3N phase, and the Mo_2C and MoO_2 phases were also detected. In this case, the Ni_2Mo_3N phase was found to be dominant at 88.7%. The difference between catalysts A and B is the aging time after drying: catalyst B was aged for 30 d after the final drying. In addition to the Ni_2Mo_3N and MoO_2 phases, the Ni crystalline phase was also detected with a content of 9.6%. Figure 1 shows that the rate of addition exerts the most influence on the formation of the Ni_2Mo_3N phase, which was most favored by a rapid rate of addition, while aging after the final drying period had no significant effect. The rapid addition of Mo/N was used in the preparation of all subsequent catalysts.

To investigate the effect of aging time when the precursor was aged before drying, two catalysts were prepared with the aging times of 0 and 1 d. Figure 2 shows the crystalline phases
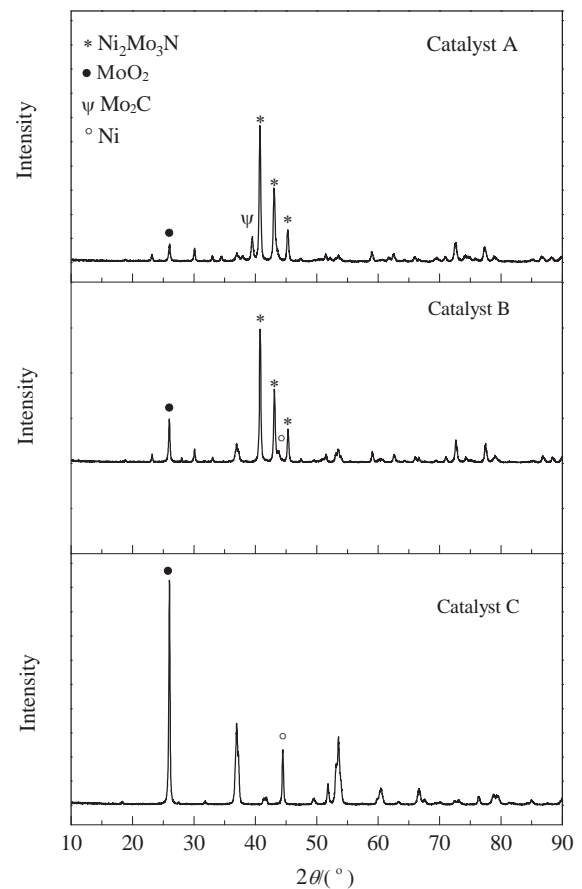

Fig. 1. XRD patterns of the Ni/Mo/N catalysts.

of the precursor and catalysts D and E. The two diffractograms at the right of Fig. 2 indicated that there was no difference in
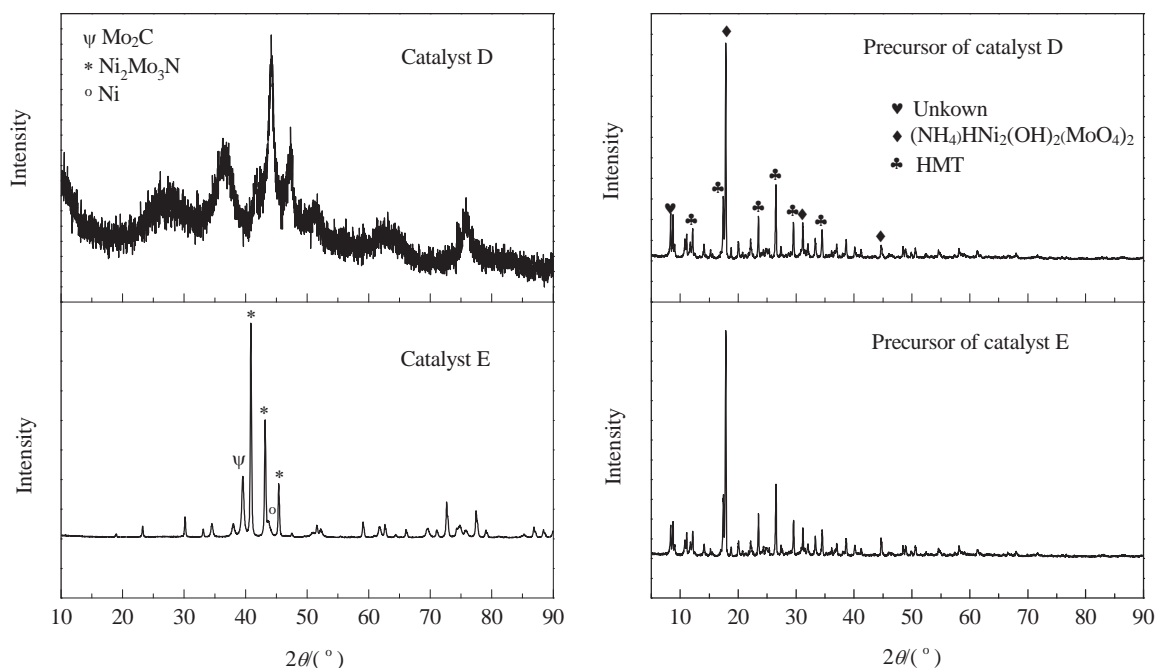

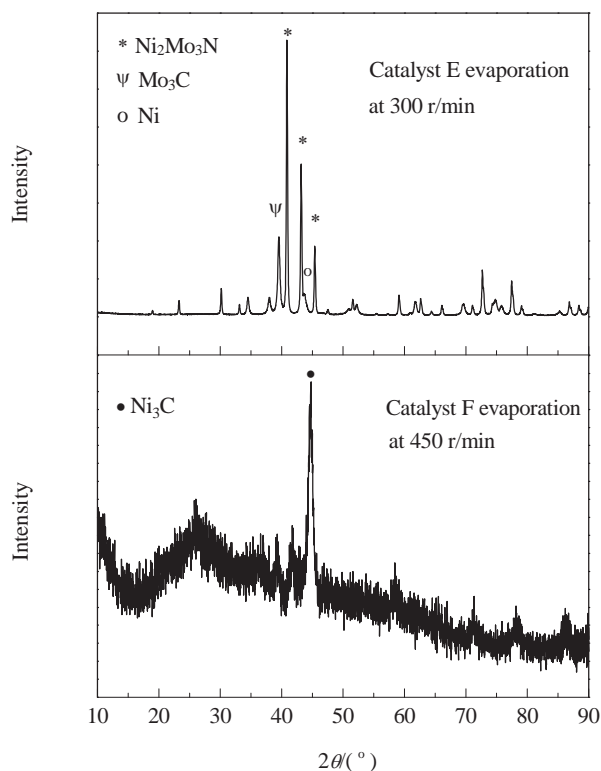**Fig. 2.** XRD patterns of catalysts D and E.

Fig. 3. XRD patterns of catalysts E and F.

Fig. 4. XRD patterns of catalyst F before and after reaction.
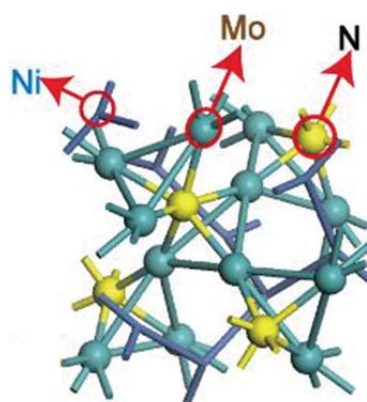
Fig. 5. The structure of the Ni_2Mo_3N catalyst.

the crystalline phases of the precursors of the D and E catalysts. The precursor phases were HMT, ammonium nickel molybdenum oxide hydroxide $((NH_4)HNi_2(OH)_2(MoO_4)_2)$, and an unknown phase. The precursor phases were different from those reported by Chouzier et al. [14]. In that paper, $(NH_4)_3H_6NiMo_6O_{24}$ was observed. Also, the Ni phase was observed in catalyst D, while the Ni_2Mo_3N phase was absent. In contrast, the peak intensities of catalyst E were high and the Ni_2Mo_3N, Mo_2C, and Ni phases were all present with contents of 57.6%, 22.54%, and 19.8%, respectively. In catalyst E, the particle size of Ni_2Mo_3N was 48.5 nm (2θ = 40.9°), and the particle sizes of Mo_2C and Ni were 22.5 nm (2θ = 39.5°) and 8.8 nm (2θ = 43.4°), respectively. The particle size of Ni_2Mo_3N was smaller than that reported by Wang et al. [16], where the particle size of Ni_2Mo_3N was found to be 52 nm when it was prepared by temperature-programmed reduction (TPR) method and 67 nm when synthesized by the decomposition of HMT. Figure 2 also illustrated that although the phase of the precursor was the same, the phases of the catalysts were not the same. There was some unknown factor that was not detectable by XRD (e.g. the release of NH_3 and H_2O) which affected the formation of Ni_2Mo_3N.

The evaporation rate was also investigated. The phases of the catalysts are shown in Fig. 3. In catalyst F synthesized under stirring at 450 r/min, the Ni_2Mo_3N phase was not detected in the XRD patterns, but a new phase, Ni_3C, was observed. Both catalysts were aged for 1 d before drying. Figure 3 showed that rapid evaporation inhibited the formation of the Ni_2Mo_3N phase.
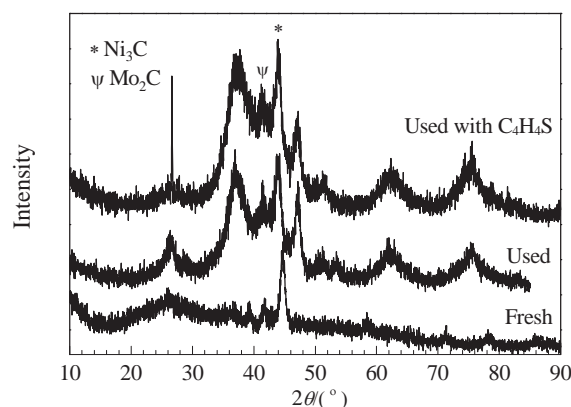
After reaction with benzene and thiophene, the XRD pattern of catalyst F showed a significant change, as shown in Fig. 4. A new phase was detected, which was Mo_2C.

The X-ray pattern of Ni_2Mo_3N is similar to that reported by Weil et al. [11] that was indexed to a primitive cubic unit cell with a lattice parameter of a = 0.66 nm and the $P4_132$ [213] space group. Other workers [9,11,13,21] have reported that Ni_2Mo_3N crystallizes in a filled β-manganese structure where a nitrogen atom is surrounded by six Mo atoms to form a slightly distorted NMo_6 octahedra. The Mo in the NMo_6 octahedra shared vertices to form a three-dimensional network. The Ni atoms formed a three-dimensional network in which each Ni atom was bonded to three adjacent Ni atoms [11]. As shown in Fig. 5, the Ni_2Mo_3N structure is generated by permeating the three-dimensional network of the NMo_6 octahedra with the three-dimensional network of Ni atoms.

TEM micrograph analysis of catalyst E, inset in Fig. 6, indicated the existence of Ni_2Mo_3N and Mo_2C. The d-spacing value for Ni_2Mo_3N (110) is 0.468 nm, which is indicated by position 1. Position 2 indicates Ni_2Mo_3N (330) with a d-spacing value of 0.156 nm. Position 3 indicates Mo_2C (101), which has a d-spacing value of 0.228 nm. The data is different from those reported in the literature [15,22]. However, these results are consistent with the XRD pattern of catalyst E. EDX showed that the atomic ratio of Ni/Mo was 5/4 when the resolution of the TEM image was 20 nm.
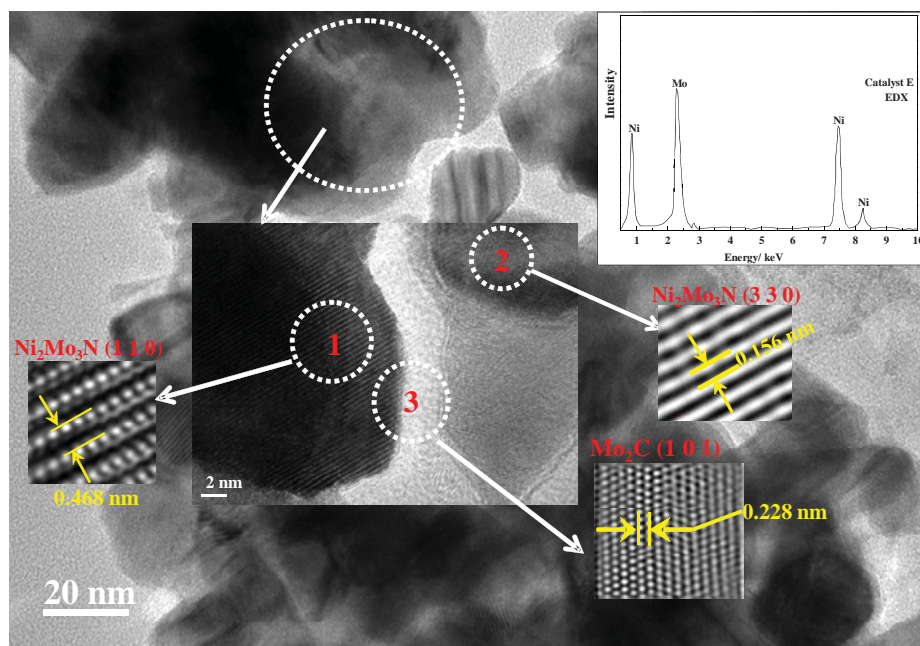
Fig. 6. TEM image of catalyst E.

3.2. Hydrogenation of benzene in absence and presence of thiophene

With the exception of catalysts B and C which were not included due to their lack of activity, the other four catalysts were evaluated in the fixed bed reactor for benzene hydrogenation in the absence of thiophene. In combination with the above XRD analysis, Fig. 7 showed that the benzene conversion of catalyst D without the Ni_2Mo_3N phase was 0. Although no Ni_2Mo_3N phase was presented in catalyst F (Table 1), the presence of Ni_3C temporarily gave it activity for benzene hydrogenation in the first four hours, after which the conversion decreased from 84% to 54%. For catalysts A and F, the MoO_2 phase was an inactive phase, while the Ni_2Mo_3N and Ni phases both gave activity. The conversion with catalyst E was the highest at 93%, and the selectivity to cyclohexane was 100%.

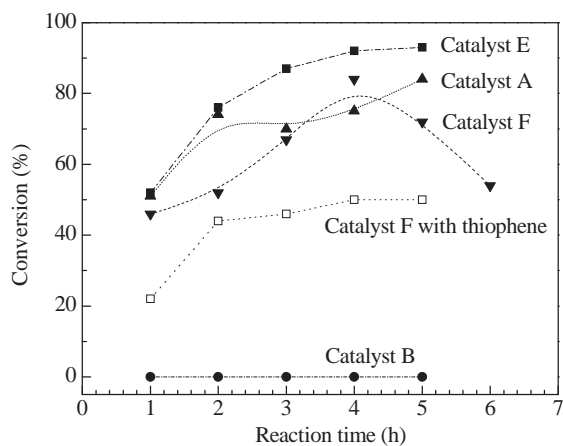Furthermore, the initial activity of catalyst F became much

Fig. 7. Benzene hydrogenation over the Ni/Mo/N catalysts.

lower and was 22% when there was 0.01 wt% thiophene in comparison with 46% benzene conversion without thiophene. However, after 4 h of hydrogenation, the conversion of benzene became constant at 50% (same value as in the absence of thiophene). The XRD pattern of catalyst F suggested that the lower initial activity was possibly due to a negative influence of the thiophene on the active site of Ni_3C, but this hypothesis requires further research. Mamède et al. [25] reported no significant change in β-Mo_2C activity (almost 100%) during 30 h reaction, which then deactivated rapidly and was inactive after 5 d when β-Mo_2C was used in the hydrogenation of toluene with 0.005% thiophene. He suggested that the surface of β-Mo_2C formed a carbosufide or MoS_2.

3.3. XPS characterization of the Ni/Mo/N catalysts

To further clarify the relationship between the chemical states of the Ni/Mo/N catalysts and their hydrogenation activity and sulfur tolerance, XPS analysis was used. The XPS spectra of Mo $3d$ for catalysts B, C, E, and catalyst E after benzene hydrogenation are shown in Fig. 8. Wei et al. [23] reported that the Mo valence state is complicated in metal nitrides and the molecular formula does not reflect the real Mo valence state. Published data and an online database (http://www.lasu rface.com/database/elementxps.php) gave the Mo $3d_{3/2}$ main peaks at 230.9 to 236.8 eV, while the binding energies of Mo $3d_{5/2}$ have a wide range from 226.1 to 235.1 eV. For catalyst E, there were three Mo valence states: Mo^{6+} ion at 235.56 and 232.31 eV (presence of MoO_3), Mo^{4+} ion at 229.61 and 232.86 eV (presence of MoO_2), and $Mo^{\delta+}$ at 228.36 and 231.36 eV (there is no reliable standard for the Mo^{2+} ion) [23]. Mamède suggested that the peak position at 228.8 eV implied the presence of molybdenum carbide. Hence, the presence of Mo_2C in
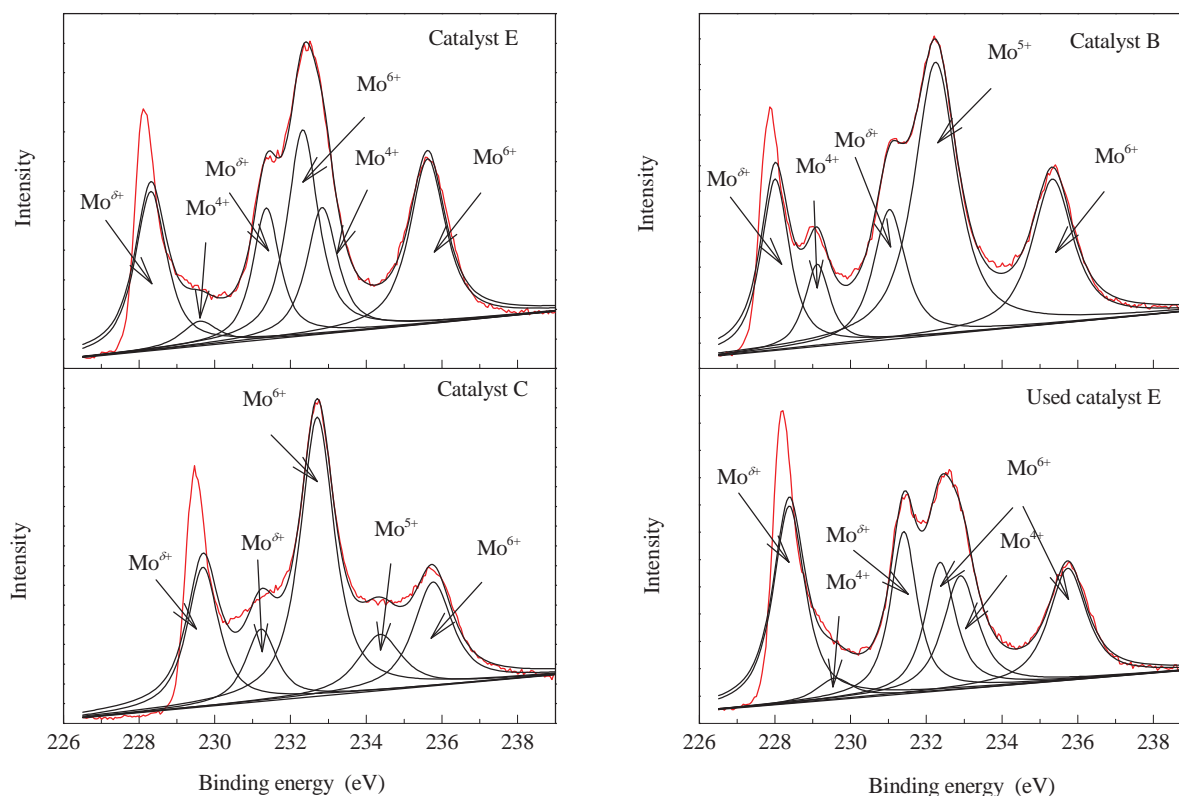
Fig. 8. Mo 3*d* XPS spectra of the Ni/Mo/N catalysts.

the catalyst E was indicated, and this was consistent with the XRD results. There was no change in the Mo valence state after catalyst E had reacted with benzene at 250 °C and 3 MPa. The Mo^{5+} ion was observed on the surface of catalysts B and C. From Figs. 6 and 8, we concluded that the Mo species in the Ni/Mo/N catalysts consisted of $Mo^{\delta+}$, Mo^{4+}, Mo^{5+}, and Mo^{6+}.

Table 2 shows that the Mo^{6+} ratio of catalyst E decreased after benzene hydrogenation, while the $Mo^{\delta+}$ and Mo^{4+} ratios increased. This implied that the Mo valence state had transformed from Mo^{6+} to $Mo^{\delta+}$ and Mo^{4+}. There were more Mo^{6+} ions in catalyst C, which led to the catalyst having the lowest catalytic activity. So, the lower chemical valence states of Mo gave the higher catalytic activity of catalyst E.

The Ni ion ratios were calculated from the deconvolution of the Ni 2*p* peak (shown in Table 3). For the three fresh catalysts, no significant difference was observed in the Ni ratio. That the Ni^0 ion ratios were the same indicated that metallic Ni was not responsible for hydrogenation activity.

In order to investigate the effect of thiophene on the catalyst, the XPS S 2*p* peak of catalyst F was analyzed. The S 2*p* XPS

spectrum consists of two peaks at 162.21 and 169.21 eV. On the basis of published data [23–25], the deconvolution of the lower binding energy peak implied the existence of two sulfur species that were assigned to the S^{2-} and S^0 species. The binding energy of 169.21 eV is characteristic of SO_4^{2-} species. Mamède et al. [25] reported that the oxidation of S^{2-} formed SO_4^{2-} species. The Mo 3*d* and Ni 2*p* XPS spectra of catalyst F after benzene hydrogenation in the presence of thiophene are shown in Fig. 9. These confirmed the formation of MoS_2 from the 228.8 eV binding energy peak after benzene hydrogenation with thiophene. In the Ni 2*p* spectra of catalyst F after reaction in the presence of thiophene, there were no Ni $2p_{3/2}$ binding energies of 852.6, 854, and 854.9 eV due to NiS, Ni_2S_3, and NiS, respectively. Therefore, we concluded that Mo_2S was responsible for the lower initial activity of Catalyst F.

4. Conclusions

A Ni_2Mo_3N catalyst was prepared by the decomposition of the HMT complex. The formation and aging of the precursors influenced the crystalline phases of the Ni_2Mo_3N catalyst. The

Table 2

Mo ion ratios from the deconvolution of the Mo 3*d* XPS peak.

Catalyst	$Mo^{\delta+}/$ Mo^{6+}	$Mo^{4+}/$ Mo^{6+}	$Mo^{5+}/$ Mo^{6+}	$Mo^{\delta+}$	Mo^{4+}	Mo^{6+}
Catalyst E fresh	0.7	0.39	—	—	—	—
Catalyst E used	1.3	0.58	—	—	—	—
Catalyst E used/fresh	—	—	—	0.75	0.94	1.40
Catalyst B fresh	1.54	0.23	1.28	—	—	—
Catalyst C fresh	0.49	—	0.19	—	—	—

Table 3

Ni ion ratio calculated by deconvolution of the Ni 2*p* peak.

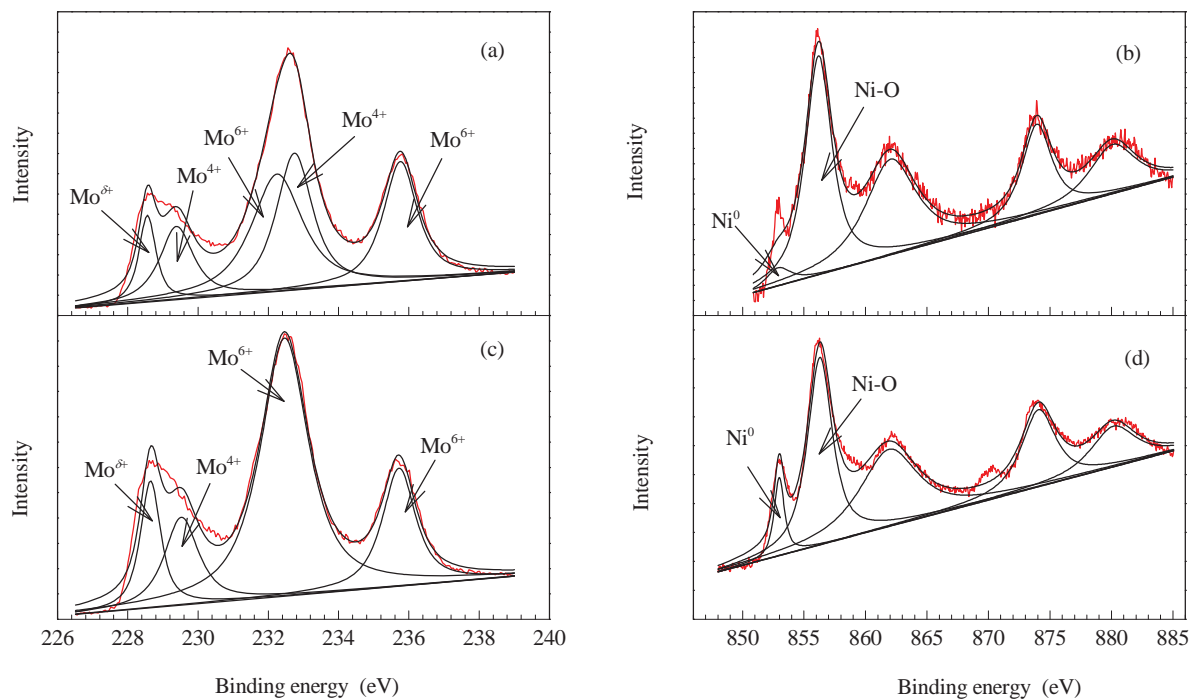| Sample	Ni^0	NiO	Ni–O
Catalyst E	0.36	—	0.60
Catalyst E used	0.41	—	0.56
Catalyst B	0.39	—	0.56
Catalyst C	0.36	0.05	0.59

Fig. 9. Mo 3*d* (a, c) and Ni 2*p* (b, d) XPS spectra for catalyst F after benzene hydrogenation. (a,b) Without C₄H₄S; (c,d) With C₄H₄S.

rapid addition of the Mo/N solution to the Ni/N solution was a significant factor in the preparation and the aging of the precursor before drying also affected catalytic activity. The Ni₂Mo₃N catalyst and the Ni₃C catalyst both gave high benzene conversion in benzene hydrogenation to 100% cyclohexane. The Ni₂Mo₃N catalyst gave a higher activity. The addition of thiophene decreased the initial hydrogenation activity because of the formation of Mo₂S.

References

[1] Fechete, I, Wang Y, Védrine J C. *Catal Today*, 2012, 189: 2
[2] EPA. http://www.epa.gov/otaq/highway-diesel/regs/ria-iv.pdf
[3] EPA. http://yosemite.epa.gov/r9/r9sips.nsf/agencyprovision/f11ad4fd00ff46f08825784000795b81/$file/section+2282.pdf?openelement
[4] Zheng J, Guo M, Song CS. *Fuel Process Technol*, 2008, 89: 467
[5] Abe J, Ma X, Song C S. Prepr. Pap.-Am. Chem. Soc., Div. Fuel Chem, 2003, 48: 609
[6] Shao J Y, Song C S. *Catal Today*, 2001, 65: 59
[7] Chen J G. *Chem Rev*, 1996, 96: 1477
[8] Chen W F, Sasaki K, Ma C, Frenkel A I, Marinkovic N, Muckerman J T, Zhu Y M, Adzic R R. *Angew Chem, Int Ed Engl*, 2012: 1
[9] Prior TJ, Battle PD. *J Solid State Chem*, 2003, 172: 138
[10] Sundaramurthy V, Dalai A K, Adjaye J. *Appl Catal A*, 2008, 335: 204
[11] Weil K S, Kumta P N, Grins J. *J Solid State Chem*, 1999, 146: 22
[12] Chouzier S, Czeri T, Roy-Auberger M, Pichon C, Geantet C, Vrinat M, Afanasiev P. *J Solid State Chem*, 2011, 184: 2668
[13] Herle P S, Hegde M S, Sooryanarayana K, Guru Row T N, Subbanna G N. *Inorg Chem*, 1998, 37: 4128
[14] Chouzier S, Afanasiev P, Vrinat M, Cseri T, Roy-Auberger M. *J Solid State Chem*, 2006, 179: 3314
[15] Wang H M, Li W, Zhang M H. *Chem Mater*, 2005, 17: 3262
[16] Wang H M. Synthesis and Hydrogenation Performance of Transition Metal Nitride Catalysts. Tianjin: Nankai University, 2006
[17] Wu Z L, Li C, Wei Z B, Ying P L, Xin Q. *J Phys Chem B*, 2002, 106: 979
[18] Agwara M O, Ndifon P T, Ndikontar M K. *Bulletin of the Chemcial Society of Ethiopia*, 2004, 18:1 43
[19] Lemmerer A. *Acta Crystall Sec B*, 2011, 67: 177
[20] Agwara M O, Yufanyi M D, Foba-Tendo J N, Atamba M A, Ndinteh D T. *J Chem Pharm Res*, 2011, 3: 196
[21] Bem D S, Gibson C P, zur Loye H C. *Chem Mater*, 1993, 5: 397
[22] Korlann S, Diaz B, Bussell M E. *Chem Mater*, 2002, 14: 4049
[23] Wei Z B, Zhao B, Grange P, Delmon B. *Appl Surf Sci*, 1998, 135: 107
[24] Guo J X, Liang J, Chu Y H, Yin H Q, Chen Y Q. *Chin J Catal* (郭家秀, 梁娟, 楚英豪, 尹华强, 陈耀强. 催化学报), 2010, 31: 278
[25] Mamède A S, Giraudon J M, Löfberg A, Leclercq L, Leclercq G. *Appl Catal A*, 2002, 227: 73
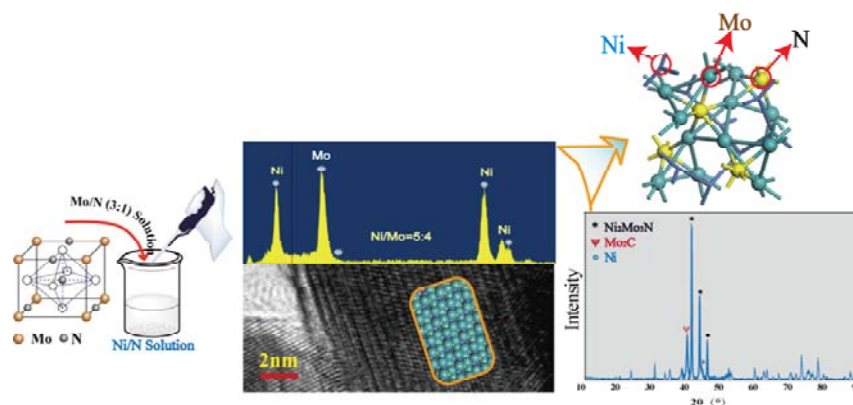
Ni/Mo/N催化剂合成及其在噻吩存在体系下苯加氢反应中的应用

褚　绮，冯　杰*，李文英，谢克昌

太原理工大学, 煤科学与技术教育部重点实验室室, 山西太原030024

Graphical Abstract

Synthesis of Ni/Mo/N catalyst and its application in benzene hydrogenation in the presence of thiophene

CHU Qi, FENG Jie*, LI Wenying, XIE Kechang
Taiyuan University of Technology

An unsupported Ni/Mo/N interstitial catalyst with high catalytic performance and sulfur tolerance is prepared by the complex decomposition of HMT at 650 °C in one pot synthesis.

摘要: Ni/Mo/N间隙型催化剂具有高的加氢活性及良好耐硫性, 可应用于煤液化油加氢精制高性能喷气燃料. N原子由于只占据晶格间隙位置, 在进入Ni/Mo过程中会因不占据晶格中的特定晶位, 容易从金属晶格溢出导致无法形成稳定的Ni/Mo/N间隙型催化剂. 为此, 本文利用前驱体晶型控制的方式来实现Ni/Mo/N催化剂合成. 采用络合物分解一步法, 考察了不同结晶过程和老化时间对合成的Ni/Mo/N催化剂用于苯加氢反应活性影响, 并采用X射线衍射、X射线光电子能谱和透射电镜-能量色散X射线光谱对催化剂结构组成进行表征. XRD分析结果显示, 钼酸铵[(NH$_4$)$_6$Mo$_7$O$_{24}$·4H$_2$O]、乙酸镍[Ni(CH$_3$COO)$_2$·4H$_2$O]和六亚甲基四胺(HMT)添加顺序、结晶过程和老化时间直接影响催化剂组成, 并决定Ni/Mo/N晶相的形成. 结晶过程慢速搅拌速度和短老化时间有利于合成含Ni$_2$Mo$_3$N, Mo$_2$C和Ni晶相的高活性Ni/Mo/N间隙型催化剂, 使苯加氢制环己烷模型反应苯的最大转化率达93%, 环己烷选择性为100%. 含0.01 wt%噻吩的存在使苯转化率由72%降至50%, XPS分析结果表明, 催化剂表面形成的MoS$_2$是催化剂活性降低的重要因素.

关键词: Ni/Mo/N催化剂; 苯加氢; 噻吩; X射线衍射; 透射电镜-能量色散X射线光谱; X射线光电子能谱